Physics of the Earth and Planetary Interiors, 30 (1982) 242–259
Elsevier Scientific Publishing Company, Amsterdam – Printed in The Netherlands

Estimation of earthquake source parameters by the inversion of waveform data: synthetic waveforms

Stuart A. Sipkin

U.S. Geological Survey, Box 25046 MS 967, Denver Federal Center, Denver, CO 80225 (U.S.A.)

(Received December 3, 1981; revision accepted March 4, 1982)

Sipkin, S.A., 1982. Estimation of earthquake source parameters by the inversion of waveform data: synthetic waveforms. Phys. Earth Planet. Inter., 30: 242–259.

Two methods are presented for the recovery of a time-dependent moment-tensor source from waveform data. One procedure utilizes multichannel signal-enhancement theory; in the other a multichannel vector-deconvolution approach, developed by Oldenburg (1982) and based on Backus–Gilbert inverse theory, is used. These methods have the advantage of being extremely flexible; both may be used either routinely or as research tools for studying particular earthquakes in detail. Both methods are also robust with respect to small errors in the Green's functions and may be used to refine estimates of source depth by minimizing the misfits to the data. The multichannel vector-deconvolution approach, although it requires more interaction, also allows a trade-off between resolution and accuracy, and complete statistics for the solution are obtained. The procedures have been tested using a number of synthetic body-wave data sets, including point and complex sources, with satisfactory results.

1. Introduction

The advent of a high-quality digital seismograph network together with recent advances in computer technology have made possible great progress in the techniques used for the quantification of seismic sources. Recently, the problem of inverting seismic waveform data to yield source parameters has received a great deal of attention, and techniques for inverting normal-mode data (Gilbert and Dziewonski, 1975; Buland and Gilbert, 1976), surface waves (McCowan, 1976; Mendiguren, 1977; Aki and Patton, 1978; Kanamori and Given, 1981), and body waves (Stump and Johnson, 1977; Strelitz, 1980; Ward, 1980b; Fitch et al., 1980; Dziewonski et al., 1981; Langston, 1981) have been presented. A review of the subject has been provided by Engdahl and Kanamori (1980).

A major stimulus to research in areas as diverse as seismic source theory, plate motion studies, seismic verification, and earthquake prediction would be provided by an on-line, semiautomated algorithm for the routine recovery of event source parameters. Particularly desirable would be a technique which could be used not only in a routine fashion, but also as a research tool for studying particular earthquakes in detail.

In this paper two methods for inverting seismic waveform data are introduced, each with different advantages and disadvantages. Although details of these methods have appeared elsewhere, neither has been applied to waveform data for these purposes. One is a "construction" method which utilizes multichannel signal-enhancement theory; the other is an "appraisal" method developed by Oldenburg (1982) which utilizes the linear inverse theory of Backus and Gilbert (1970). Both methods rely upon the moment-tensor representation of seismic sources and are based on the linear rela-

0031-9201/82/0000–0000/$02.75

tionship between the elements of the moment tensor and the seismogram (Gilbert, 1971). Employing the multichannel signal-enhancement approach, the Green's functions are considered to be the multichannel input, the moment rate tensor is viewed as the convolution filter operating on the input, and the observed seismograms are the desired output. Using recursion techniques, the elements of the moment rate tensor are solved for as the optimum (in a least-squares sense) multichannel signal-enhancement filter. This method allows each element of the moment rate tensor to be an independent function of time; in addition, the duration of the source time function can be constrained by limiting the length of the filter. For example, the best-fitting point source in time may be found by limiting the filter to a length of one. Linear constraints, such as seeking a completely deviatoric source, can easily be incorporated by either reparameterizing the convolution equation or by including the equations of constraint with the normal equations.

In the second approach, a multichannel vector-deconvolution method developed by Oldenburg (1982) and based on Backus–Gilbert inverse theory is used. In this approach, a set of filters is computed which, when convolved with the data, yield unique time averages of the individual elements of the moment rate tensor. For each element this average is the true time-history convolved with a primary averaging function plus contamination from secondary averaging functions convolved with the other elements of the moment rate tensor. However, by chosing a suitable set of weights, these secondary averaging functions can be annihilated. This approach allows unique time averages of the elements of the moment rate tensor to be obtained, as well as their statistical errors and estimates of the available resolution; it also allows a trade-off between resolution and accuracy.

The advantages of these two methods include their being more flexible than many other algorithms; i.e., they can be used either in a routine fashion, for example to find the best-fitting point source, or to study the details of a complex event. Furthermore, the use of these methods is not limited to the study of teleseismically recorded long-period body waves; any waveform data, recorded in any frequency band, for which the appropriate Green's functions can be computed could theoretically be inverted. In addition, as we shall show, these methods are robust with respect to minor errors in the Green's functions. In this paper the two methods are outlined and tests using synthetic body-wave data are presented.

2. Moment-tensor representation

Central to any linear inversion of waveform data for the seismic source is the concept of the moment tensor. This representation was first proposed by Gilbert (1971) for studying the free oscillations of the Earth. Since then, techniques for the inversion of seismic signals have been formulated for free-oscillation, surface-wave, and body-wave data (see Section 1). Using a moment-tensor representation for body waves (Aki and Richards, 1980, p. 52), the displacement field may be written as

$$u_j(\mathbf{r},t) = \iint_{\Sigma} M_{kl}(\mathbf{r}_0,t) * G_{jk,l}(\mathbf{r},t;\, \mathbf{r}_0,0)\, \mathrm{d}\Sigma$$
$$j = 1,\ldots,N$$

where M_{kl} are the components of the moment-density tensor, $G_{jk,l}$ are the elastodynamic Green's functions, $\mathbf{r}$ is the position of the receiver, $\mathbf{r}_0$ is a point on the fault surface, and $\mathrm{d}\Sigma$ is an element on the fault surface Σ. When considering only wavelengths for which Σ is effectively a point source, the entire surface may be considered to be a system of couples operating at a point. The moment tensor is then defined as

$$\mathrm{M}_{kl}(t) = \iint_{\Sigma} M_{kl}(\mathbf{r}_0,t)\, \mathrm{d}\Sigma$$

and

$$u_j(\mathbf{r},t) = \mathrm{M}_{kl}(t) * G_{jk,l}(\mathbf{r},t;\, \hat{\mathbf{r}}_0,0) \qquad (1)$$
$$j = 1,\ldots,N$$

where $\hat{\mathbf{r}}_0$ is the centroid of Σ. In general, this equation contains terms in both M_{kl} and $\dot{\mathrm{M}}_{kl}$ (where a superscript dot denotes the time derivative) (Aki and Richards, 1980, p. 79); however,

owing to the distance-dependence of these terms and to the symmetry of $\dot{M}_{kl}$, eq. (1) reduces, in the far field, to

$$u_j(\mathbf{r},t) = \sum_{k=1}^{6} m_k(t) * g_{jk}(\mathbf{r},t;\hat{\mathbf{r}}_0,0) \quad j=1,\ldots,N \tag{2}$$

where $\mathbf{m}(t)$ is the vector containing the six independent elements of the moment rate tensor, i.e.,

$$m_1(t) = \dot{M}_{11}(t) \qquad m_4(t) = \dot{M}_{13}(t)$$
$$m_2(t) = \dot{M}_{12}(t) \qquad m_5(t) = \dot{M}_{23}(t)$$
$$m_3(t) = \dot{M}_{22}(t) \qquad m_6(t) = \dot{M}_{33}(t)$$

and the g_{jk} are the corresponding Green's functions. It is this linear relationship upon which most inversion schemes depend.

In practice, it is not necessary to compute each of the six Green's functions individually. Any far-field P-wave seismogram can be written as a linear combination of three "fundamental solutions", or seismograms, which depend only on take-off angle, or equivalently, ray parameter (Aki and Richards, 1980, p. 467; Ward, 1980a, b). The coefficients by which these three fundamental seismograms are multiplied are made up of products of each of the elements of the moment rate tensor and a trigonometric function which depends only on the azimuth from the source to the receiver. Thus the six Green's functions can be found by computing the three fundamental seismograms and multiplying them by the appropriate trigonometric functions. The fundamental seismograms may be computed using any available algorithm; in this paper the WKBJ method (Chapman, 1978; Dey-Sarkar and Chapman, 1978) is used.

Since, for now, only earthquakes will be studied, some constraints may be incorporated into the system of equations. The constraint that the source be a double couple is nonlinear and will not be used. However, the constraint that the source be purely deviatoric [$\mathrm{tr}(\dot{\mathbf{M}}) = 0$] is linear and is easily imposed. This can be done either by including the equation of constraint in the normal equations or by reparameterizing eq. (2):

$$u_j(\mathbf{r},t) = \sum_{k=1}^{5} m_k(t) * g'_{jk}(\mathbf{r},t;\hat{\mathbf{r}}_0,0) \quad j=1,\ldots,N$$

where

$$g'_{jk} = \begin{cases} g_{jk} - g_{j6} & k = 1,3 \\ g_{jk} & k = 2,4,5 \end{cases}$$

After carrying out the inversion, the moment rate tensor may be examined, or the moment tensor found by numerical integration. The moment tensor can then be decomposed in terms of its principal axes for each point in time. Since the solutions are not restricted to be double couples the intermediate eigenvalues will not necessarily be equal to zero. If desired, the moment tensors may also be decomposed into the best-fitting double couples, the remainders being compensated linear-vector dipoles (CLVD's). In all of the synthetic tests these remainders are negligible, and in tests on real data are found to be small (Sipkin, 1981).

If these algorithms were to be applied to explosion or questionable data, the constraint that the source be purely deviatoric should not be used. This constraint could also be dropped if it was desired to investigate a suspected isotropic component of a source (e.g., Gilbert and Dziewonski, 1975).

3. Multichannel signal enhancement

The general case of multichannel input and multichannel output can, for this problem, be reduced to the special case of single-channel output. Equation (2) may then be rewritten as

$$\hat{u}(t) = \sum_{k=1}^{6} m_k(t) * \hat{g}_k(t) + n(t)$$

where $\hat{u}(t)$ and $\hat{\mathbf{g}}(t)$ are the time series formed by concatenating the N seismograms $u_j(\mathbf{r},t)$ and the N Green's functions $g_{jk}(\mathbf{r}, t; \hat{\mathbf{r}}_0, 0)$; $\hat{u}(t)$ is now the desired single-channel output, $\hat{\mathbf{g}}(t)$ is the multichannel (six channels) input, $\mathbf{m}(t)$ is the convolution filter operating on the input, and $n(t)$ is an estimate of the noise. Following Claerbout (1976), this convolution equation may then be written in matrix form as

$$\begin{bmatrix} \hat{u}(0) \\ \hat{u}(t_1) \\ \hat{u}(t_2) \\ \vdots \end{bmatrix} = \begin{bmatrix} \hat{g}_1(0) & \hat{g}_2(0) & \dots & \hat{g}_6(0) & 0 & \dots & & \\ \hat{g}_1(t_1) & \hat{g}_2(t_1) & \dots & \hat{g}_6(t_1) & \hat{g}_1(0) & \dots & \hat{g}_6(0)0 & \dots \\ \hat{g}_1(t_2) & \hat{g}_2(t_2) & \dots & \hat{g}_6(t_2) & \hat{g}_1(t_1) & \dots & \hat{g}_6(t_1) & \dots \\ \vdots & \vdots & & \vdots & \hat{g}_1(t_2) & \dots & \hat{g}_6(t_2) & \dots \\ & & & & \vdots & & \vdots & \end{bmatrix} \begin{bmatrix} m_1(0) \\ m_2(0) \\ \vdots \\ m_6(0) \\ m_1(t_1) \\ \vdots \\ m_6(t_1) \\ \vdots \end{bmatrix}$$

or

$$\hat{\mathbf{u}} = \hat{\mathbf{G}}\hat{\mathbf{m}}$$

The standard least-squares solution to this system of equations is

$$\hat{\mathbf{m}} = (\hat{\mathbf{G}}^{\mathrm{T}}\hat{\mathbf{G}})^{-1}\hat{\mathbf{G}}^{\mathrm{T}}\hat{\mathbf{u}}$$

Given the size of $\hat{\mathbf{G}}$, solving this equation would be an imposing task were it not for certain symmetries present. In order to take advantage of these symmetries, the auto- and cross-correlation operators are introduced:

$$a_{ij}(s) = \sum_t \hat{g}_i(t)\hat{g}_j(t+s)$$

$$c_i(s) = \sum_t \hat{g}_i(t)\hat{u}(t+s)$$

Then

$$\hat{\mathbf{G}}^{\mathrm{T}}\hat{\mathbf{u}} = [c_1(0)\dots c_6(0) \quad c_1(t_1)\dots c_6(t_1)\dots]^{\mathrm{T}} = \mathbf{c}$$

and

$$\hat{\mathbf{G}}^{\mathrm{T}}\hat{\mathbf{G}} = \mathbf{A} = \begin{bmatrix} a_{11}(0) & \dots & a_{16}(0) & a_{11}(-1) & \dots & a_{16}(-1) & a_{11}(-2) & \dots & a_{16}(-2) & \dots \\ \vdots & & \vdots & \vdots & & \vdots & \vdots & & \vdots & \\ a_{61}(0) & \dots & a_{66}(0) & a_{61}(-1) & \dots & a_{66}(-1) & a_{61}(-2) & \dots & a_{66}(-2) & \dots \\ a_{11}(1) & \dots & a_{16}(1) & a_{11}(0) & \dots & a_{16}(0) & a_{11}(-1) & \dots & a_{16}(-1) & \dots \\ \vdots & & \vdots & \vdots & & \vdots & \vdots & & \vdots & \\ a_{61}(1) & \dots & a_{66}(1) & a_{61}(0) & \dots & a_{66}(0) & a_{61}(-1) & \dots & a_{66}(-1) & \dots \\ a_{11}(2) & \dots & a_{16}(2) & a_{11}(1) & \dots & a_{61}(1) & a_{11}(0) & \dots & a_{61}(0) & \dots \\ \vdots & & \vdots & \vdots & & \vdots & \vdots & & \vdots & \\ a_{61}(2) & \dots & a_{66}(2) & a_{61}(1) & \dots & a_{66}(1) & a_{61}(0) & \dots & a_{66}(0) & \dots \\ \vdots & & \vdots & \vdots & & \vdots & \vdots & & \vdots & \end{bmatrix}$$

Then define the submatrix blocks

$$\tilde{\mathbf{A}}(\tau) = \begin{bmatrix} a_{11}(\tau) & \dots & a_{61}(\tau) \\ \vdots & & \vdots \\ a_{61}(\tau) & \dots & a_{66}(\tau) \end{bmatrix} = \tilde{\mathbf{A}}^{\mathrm{T}}(-\tau)$$

so that

$$\mathbf{A} = \begin{bmatrix} \tilde{\mathbf{A}}(0) & \tilde{\mathbf{A}}(-1) & \tilde{\mathbf{A}}(-2) & \dots \\ \tilde{\mathbf{A}}(1) & \tilde{\mathbf{A}}(0) & \tilde{\mathbf{A}}(-1) & \dots \\ \tilde{\mathbf{A}}(2) & \tilde{\mathbf{A}}(1) & \tilde{\mathbf{A}}(0) & \dots \\ \vdots & \vdots & \vdots & \end{bmatrix}$$

Using this notation, the normal equations, in matrix form, are

$$\mathbf{A}\hat{\mathbf{m}} = \mathbf{c}$$

The matrix **A** is in the form of a "block Toepliz" matrix, so this system of equations may be quickly solved using recursive techniques. These techniques are equivalent to using recurrence relations in orthogonal polynomial theory. The savings in both time and storage necessary are possible because **A** has only N different elements, whereas a general matrix could have up to N^2 elements. The details of these recursive techniques can be found elsewhere (Robinson, 1967; Claerbout, 1976; Oppenheim, 1978) and are not discussed here.

After the inversion has been performed the amount of misfit between the output and the original data is measured by the normalized mean-square error (NMSE). Unfortunately, since this is a "construction" technique it is difficult to obtain formal estimates of the variances of the individual elements of the moment tensor. However, by using an "appraisal" method a complete statistical analysis can be performed. The following Section describes such a technique.

4. Multichannel vector deconvolution

The technique discussed in this Section was developed by Oldenburg (1982) as an extension of his single-channel scalar-deconvolution method (Oldenburg, 1981). Following Oldenburg (1982), we wish to find a set of filters $v_{lj}(t)$ such that averages $\langle m_l(t)\rangle$ of the lth model component are obtained when these filters are convolved with the N seismograms, or data channels:

$$\langle m_l(t)\rangle = \sum_{j=1}^{N} v_{lj}(t) * u_j(t) \tag{3}$$

Substituting eq. (2) into (3) yields

$$\langle m_l(t)\rangle = \sum_{j=1}^{N} v_{lj} * \left[\sum_{k=1}^{6} m_k(t) * g_{jk}(t) + n_j(t) \right]$$

$$= \sum_{k=1}^{6} m_k(t) * a_{lk}(t) + e\langle m_l(t)\rangle$$

where

$$a_{lk}(t) = \sum_{j=1}^{N} v_{lj}(t) * g_{jk}(t)$$

$$e\langle m_l(t)\rangle = \sum_{j=1}^{N} v_{lj} * n_j(t)$$

$a_{ll}(t)$ is the "primary" averaging function, the $a_{lk}(t)$ are the "secondary" averaging functions, $e\langle m_l(t)\rangle$ is the error in $\langle m_l(t)\rangle$, and $n_j(t)$ is an estimate of the noise in the jth seismogram. In order to interpret the averages, the secondary averaging functions must be made sufficiently small. Then

$$\langle m_l(t)\rangle \simeq m_l(t) * a_{ll}(t) + e\langle m_l(t)\rangle$$

This result will be achieved if

$$a_{ll}(t) = \sum_{j=1}^{N} v_{lj}(t) * g_{jl}(t) = h(t) \tag{4a}$$

$$a_{lk}(t) = \sum_{j=1}^{N} v_{lj}(t) * g_{jk}(t) \simeq 0 \qquad k \neq l \tag{4b}$$

where $h(t)$ is a delta-like function. The squared difference between the left- and right-hand sides of eqs. (4a) and (4b) is

$$\phi_l = \int_{-T/2}^{T/2} |a_{ll}(t) - h(t)|^2 \, \mathrm{d}t + \sum_{\substack{k=1 \\ k \neq l}}^{6} w_{lk} \int_{-T/2}^{T/2} |a_{lk}(t)|^2 \, \mathrm{d}t \tag{5}$$

where the w_{lk} are a set of arbitrary weights used to reduce the amplitudes of the secondary averaging functions, and T is the total length of the averaging functions. Then, by using the Kroniker delta and introducing the statistical variance of the averages and the trade-off parameter θ, the two terms in eq. (5) may be contracted and the desired quadratic form obtained:

$$\phi_l = \cos\theta \sum_{k=1}^{6} w_{lk} \int_{-T/2}^{T/2} |a_{lk}(t) - h(t)\delta_{lk}|^2 \, \mathrm{d}t + \sin\theta \, \mathrm{var}\, e\langle m_l(t)\rangle$$

The trade-off parameter allows resolution to be traded off for increased accuracy. For a given

value of θ, it is then required to find the filters $v_{lj}(t)$ which minimize ϕ_l. The details of this proce-dure have been given by Oldenburg (1982). These filters are then used to compute the averaging functions and the averages of the model components.

It should be stressed that the averages of the elements of the moment rate tensor will not, in general, reproduce the data when convolved with the Green's functions. They are, however, unique in that all time-dependent moment rate tensors which reproduce the data will have the same averages when convolved with the appropriate averaging functions. Unless there is additional information, or a priori assumptions concerning the source time history, these averages completely summarize our knowledge about the moment rate tensor. If, however, there exists additional information about the functional form of the source time history then this can be used in interpreting the results of the inversion. If it is assumed, for example, that the event being studied is a complex event composed of discrete subevents, the averages of the elements of the moment rate tensor should appear to be replications of the appropriate averaging functions displaced in time, with different amplitudes. Given the pass band of the long-period SRO channel, the resolution width will probably be greater than the length of the source time functions for the individual subevents; thus the "true" model should be a series of delta functions. In principle, the delays t_i and amplitudes A_{il} of the M subevents could be found by minimizing

$$\psi = \sum_{j=1}^{N} \sum_{k=1}^{N_t} \sum_{l=1}^{6} \left[\sum_{i=1}^{M} A_{il} g_{jl}(t_i - t_k) - u_j(t_k) \right]^2$$

where N_t is the number of time points in each seismogram. Unfortunately, this minimization is nonlinear and must be solved using an iterative approach. This requires a starting solution, which in turn requires knowledge of M, the number of delta functions needed to adequately describe the model. This can rarely be established from an examination of the data.

An alternate procedure (Oldenburg, 1981) is based on the fact that the model averages are linear combinations of the translated averaging functions. The function to be minimized is then

$$\chi = \sum_{l=1}^{6} \sum_{k=1}^{N_t} \left[\sum_{i=1}^{M} A_{il} a_{ll}(t_i - t_k) - \langle m_l(t_k) \rangle \right]^2$$

The advantage of this is that from an examination of the averages it is possible to determine the number of resolved peaks and obtain a good approximation of the amplitudes and time delays. This, then, is the starting model. If the standard deviation of each $\langle m_l(t) \rangle$ is σ_l, then

$$E[\chi] = N_t \sum_{l=1}^{6} \sigma_l^2$$

where $E[\ ]$ denotes expected value. If χ is significantly larger than its expected value then either the wrong number of peaks has been estimated from the averages, or the minimization has converged on a local minimum because the starting model was poor. The latter possibility is another reason that minimizing χ is a better procedure than minimizing ψ; the averaging functions are narrower in time than the Green's functions, thus reducing the chances of converging on a local minimum.

5. Synthetic seismograms

For the purposes of testing the two algorithms, synthetic seismograms and Green's functions were computed using the WKBJ method and model 1066B (Gilbert and Dziewonski, 1975). Both the seismograms and Green's functions are of composite P waves consisting of P, pP, and sP, with attenuation introduced via a time-domain operator having $t^* = 1$. The instrument response is that of the long-period SRO channel. The experiment was conducted for three different source types at two depths, one shallow (33 km), the other deep (520 km). The three sources considered were a simple double-couple source which is a point in both time and space; two double-couple point sources having the same orientation but displaced in time; and two double-couple point sources displaced in time but having different orientations. The results for the two complex sources were similar, so only the latter are discussed. In these synthetic experi-

ments there are, of course, no problems due to travel times being perturbed by lateral variations in Earth structure or by event mislocation. When considering real data, however, something must be done to negate these effects. Since it is often difficult to locate the first break on a long-period record, we have chosen to do this by aligning the signal envelopes. That is, for each seismogram the envelope of the signal is computed and the seismogram is then shifted in time so that the first peak in its envelope is aligned with the others. Tests using the synthetic data sets indicate that this procedure is effective for removing travel-time deviations.

5.1. Simple source

The point source considered was a pure thrust event striking due north and dipping 45° to the east, with a step-function source time history (delta-function far-field source time function). For each of the two source depths ten synthetic seismograms at various distances and azimuths were computed, together with the corresponding Green's functions. The seismograms and some of the Green's functions computed for the source depth of 33 km are shown in Figs. 1 and 2. The orientation chosen is a severe test for the inversion procedures since, for teleseismic distances, the P waves all leave the focal sphere from the same quadrant and all of the waveforms are similar. The multichannel signal-enhancement algorithm was tested both with and without the constraint that the solution be a point source in time. For the case of perfect data, the correct solutions were obtained exactly, both with and without the constraint being imposed, with negligible normalized mean-square errors. When 5–10% Gaussian random noise was added to the data there was a very slight deterioration in the solutions; when inverting for a point source the orientations and scalar moments were in error by less than 1% (Table I, Fig. 3). When the unconstrained solutions were decomposed into their principal axes, the orientations as functions of time were almost constant and the scalar moments were in error by less than 10% (Fig. 4). The amounts of misfit for the constrained and unconstrained solutions were almost the same (NMSE of

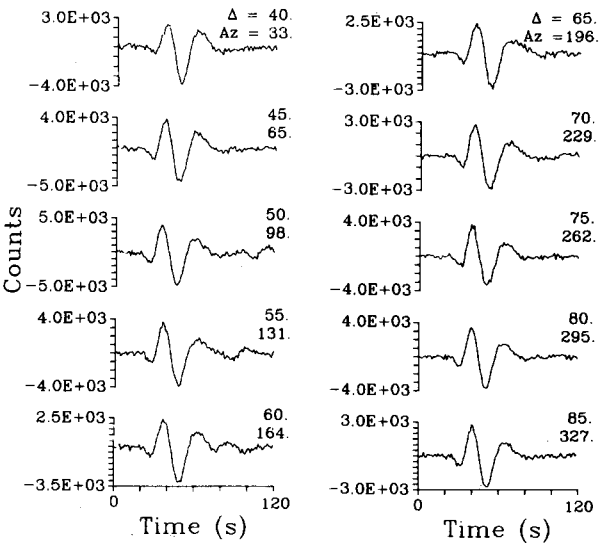

Fig. 1. Synthetic P waves for simple source (strike 0°, dip 45°, slip 90°, depth 33 km). The waveforms include P, pP, and sP. 5–10% Gaussian random noise has been added.

0.041 and 0.034, respectively, for the deep event, and 0.014 and 0.011, respectively, for the shallow event), indicating that allowing a finite source duration did not significantly improve the fit to the data. The values given in Tables I and II for

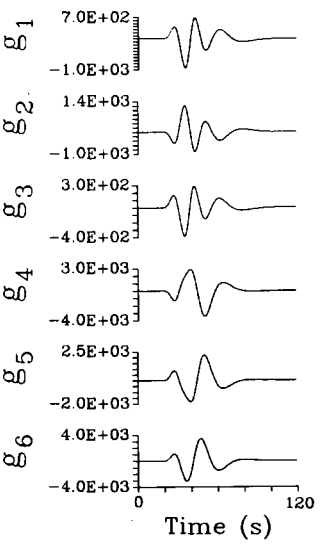

Fig. 2. Green's functions for the first P wave shown in Fig. 1.

TABLE I

Simple-source double-couple parameters

	Scalar moment ($\times 10^{25}$)	Strike (deg.)	Dip (deg.)	Slip (deg.)	P		T		B		Misfit
					Az. (deg.)	Plunge (deg.)	Az. (deg.)	Plunge (deg.)	Az. (deg.)	Plunge (deg.)	
Correct solution	1.0	0/360	45	90	90/270	0	0/180	90	180/0	0	–
Multichannel signal enhancement											
True source depth = 33 km											
$h = 33$											
point in time	1.0	359	45	89	270	0	183	89	0	1	0.014 [b]
finite duration [a]	1.0	355	46	85	88	1	193	86	358	3	0.011
$h = 44$											
point in time	0.8	351	44	73	273	2	174	78	3	12	0.397
finite duration	1.4	8	49	99	92	4	332	82	182	7	0.082
True source depth = 520 km											
$h = 520$											
point in time	1.0	0	45	90	90	0	72	90	180	0	0.041
finite duration	1.1	5	45	95	91	0	0	86	181	4	0.034
$h = 532$											
point in time	1.0	0	45	91	270	0	25	90	180	0	0.043
finite duration	1.1	6	45	96	92	0	0	86	182	4	0.034
Deconvolution											
True source depth = 33 km											
$h = 33$	1.1	0	45	90	90	0	0	90	180	0	0.053/0.093 [c]
$h = 44$	1.0	0	45	90	90	0	0	90	180	0	0.491/0.103
True source depth = 520 km											
$h = 520$	0.9	0	45	90	90	0	0	90	180	0	0.051/0.082
$h = 532$	0.9	0	45	90	90	0	0	90	180	0	0.053/0.082

[a] Parameters for time at which $\|\dot{\mathbf{M}}(t)\|$ is a maximum.

[b] Normalized mean-square error.

[c] $\chi/E[\chi]$.

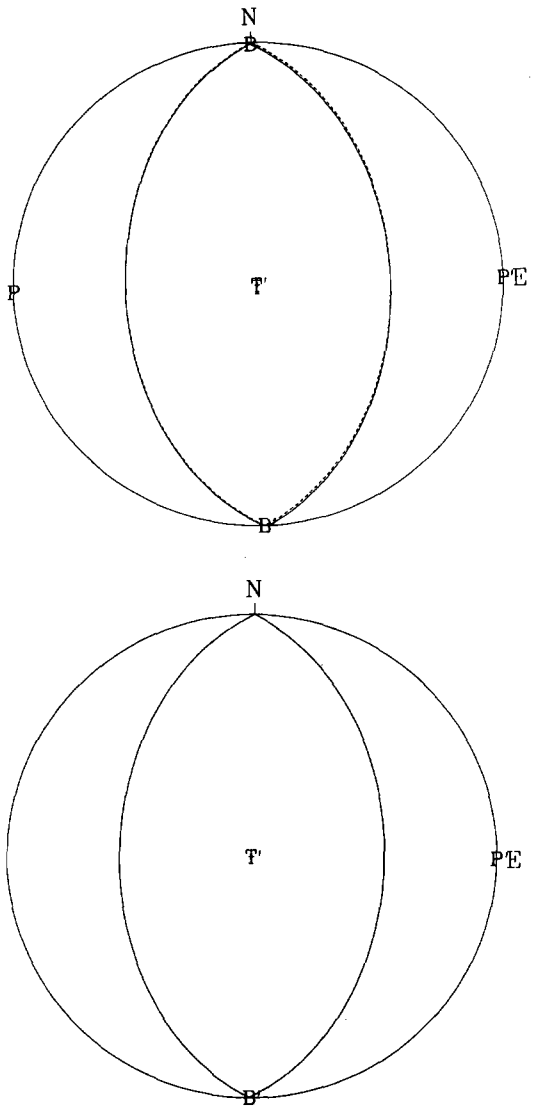

Fig. 3. Nodal-plane solutions for the simple-source data sets obtained by decomposition of the moment-tensor solutions. Solid lines are the inversion results, dashed lines are the correct solutions: (a) source depth 33 km; (b) source depth 520 km.

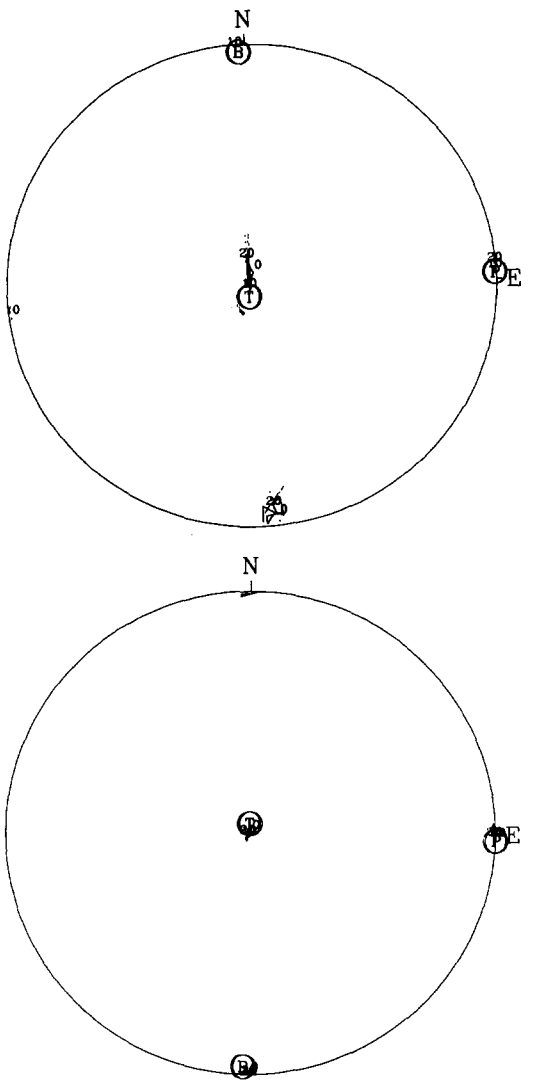

Fig. 4. Principal axes as functions of time for the simple-source data sets obtained by decomposition of the moment-tensor solutions. Numbers of seconds after initial rupture are indicated. Circled P, T, B indicate orientation at time when $\|\dot{\mathbf{M}}(t)\|$ is a maximum: (a) source depth 33 km; (b) source depth 520 km.

the finite-duration solutions are those which correspond to the time at which the scalar norm of the moment rate tensor is a maximum.

The sensitivity of this method to errors in the Green's functions was tested by performing the inversions using Green's functions computed for the wrong depths. Epicentral location errors will result in errors in the distances and will change the waveforms only slightly. However, errors in the estimated depth will have a significant influence on the Green's functions for shallow events, owing to differences in the time delays of pP and sP

TABLE II

Complex-source double-couple parameters: cumulative solutions

	Scalar moment ($\times 10^{25}$)	Strike (deg.)	Dip (deg.)	Slip (deg.)	P		T		B		Misfit
					Az. (deg.)	Plunge (deg.)	Az. (deg.)	Plunge (deg.)	Az. (deg.)	Plunge (deg.)	
Correct solution	1.7	0/360	60	90	90	15	270	75	0/180	0	–
Multichannel signal enhancement											
True source depth = 33 km											
$h = 33$											
point in time	0.9	9	63	103	90	18	305	69	184	11	0.348 [b]
finite duration [a]	1.7	353	64	95	79	19	274	70	170	5	0.015
$h = 44$											
point in time	0.51	348	54	76	89	8	212	76	357	11	0.743
finite duration	1.6	41	64	102	122	18	335	68	216	11	0.153
True source depth = 520 km											
$h = 520$											
point in time	0.8	2	63	91	91	18	274	72	181	1	0.420
finite duration	1.9	358	60	88	89	15	261	75	359	2	0.024
$h = 532$											
point in time	0.9	358	59	88	89	14	263	76	359	1	0.500
finite duration	1.9	359	60	88	90	15	264	75	0	1	0.026
Deconvolution											
True source depth = 33 km											
$h = 33$	1.6	0	62	90	90	17	270	73	0	0	0.080/0.088 [c]
$h = 44$	1.4	327	61	92	56	16	241	74	146	1	0.339/0.056
True source depth = 520 km											
$h = 520$	1.7	0	62	90	90	17	270	73	0	0	0.076/0.083
$h = 532$	1.6	0	63	90	90	18	270	72	0	0	0.080/0.083

[a] Parameters for time at which $\|\dot{\mathbf{M}}(t)\|$ is a maximum.

[b] Normalized mean-square error.

[c] $\chi / E[\chi]$.

relative to P. The result of these differences can be seen in the inversion results obtained when the Green's functions were computed using a source depth different from that used to compute the synthetic seismograms (Table I). When the seismograms were computed using a source depth of 520 km, but a depth of 532 km was assumed when computing the Green's functions, the inversion results were virtually unchanged from those obtained when the correct source depth was used (Fig. 5b), and the misfit was only slightly greater. This is because the pP and sP arrivals are outside the time window used. However, when the actual source depth was 33 km, but a depth of 44 km was used to compute the Green's functions, the misfit when the source was constrained to be a point in time was almost thirty times greater than when the correct source depth was used. The encouraging fact is that the source geometry obtained was still very close to the correct solution (Fig. 5a), none of the parameters being in error by more than 5%. These tests imply that this technique is fairly robust with respect to hypocentral mislocation and to small errors in the Earth model used to compute the Green's functions. They also indicate that the source depth may be refined by finding the depth for which the misfit to the data is minimized.

Similar results were obtained using the multichannel vector-deconvolution method. An example of the primary averaging functions and averages of the moment rate tensor are shown in Fig. 6. The horizontal lines in Fig. 6b indicate the $\pm 1\sigma$ levels. Only $\langle m_1(t)\rangle$ and $\langle m_6(t)\rangle$ have peaks above the indicated background noise; variations in the other components are approximately equal to the computed noise level. It can easily be seen that the averages are simple replications of the primary averaging functions. When the best-fitting delta functions were found using the iterative technique discussed in Section 4, the results shown in Table I were obtained. Figure 7 displays the nodal-plane solution and the error ellipses for the principal axes. As for the multichannel signal-enhancement algorithm, even when the source depth used to compute the Green's functions was too deep by more than 10 km an essentially correct solution was still obtained, but with a larger misfit. And again, for the 520 km deep source the misfit

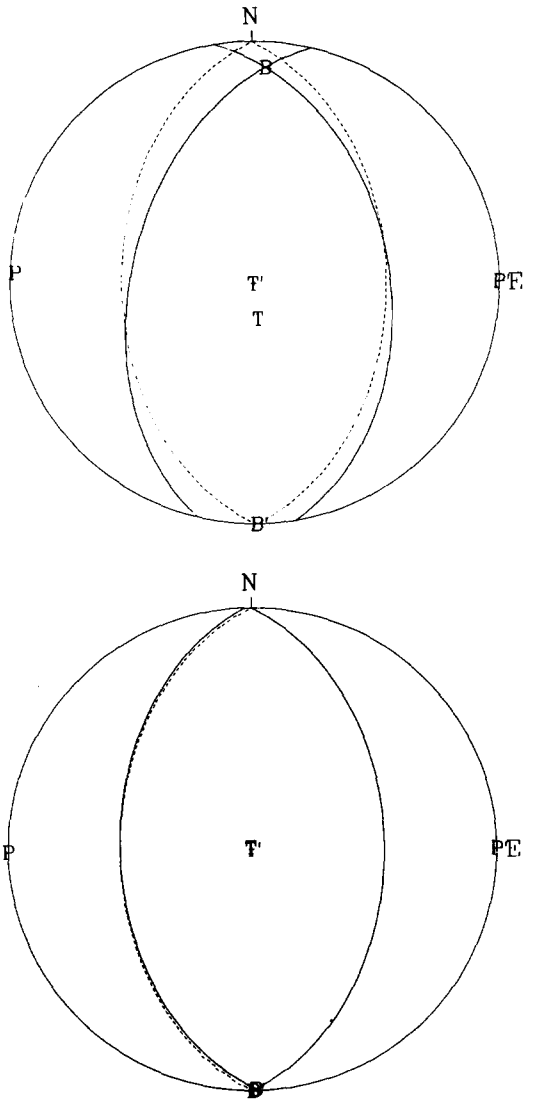

Fig. 5. Nodal-plane solutions for the simple-source data sets obtained using Green's functions computed for the wrong depths. Conventions as in Fig. 3: (a) source depth 33 km, Green's functions for source 44 km deep; (b) source depth 520 km, Green's functions for source 532 km deep.

was only slightly greater, whereas for the 33 km deep source the misfit was significantly greater. The other statistics also reflect errors in the assumed source depth. The standard deviations found for the elements of the moment rate tensor, and thus the error ellipses for the principal axes,

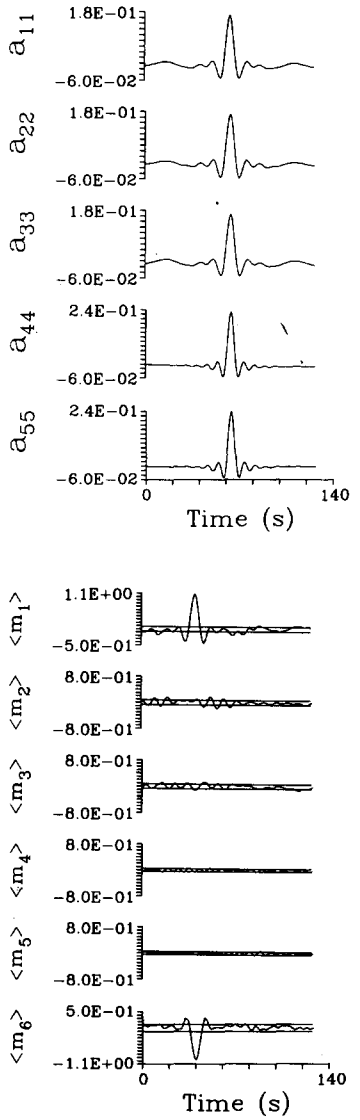

Fig. 6. (a) Primary averaging functions and (b) moment-rate-tensor averages for the simple-source data set with a source depth of 33 km. Horizontal lines indicate $\pm 1\sigma$ levels.

are larger for the case of incorrect source depth. These facts are not unexpected, since Oldenburg (1981) showed, for the single-channel scalar-deconvolution problem, that by using only an approximate kernel function reasonable results may still be obtained, but with an increased variance. The same phenomenon will be observed when

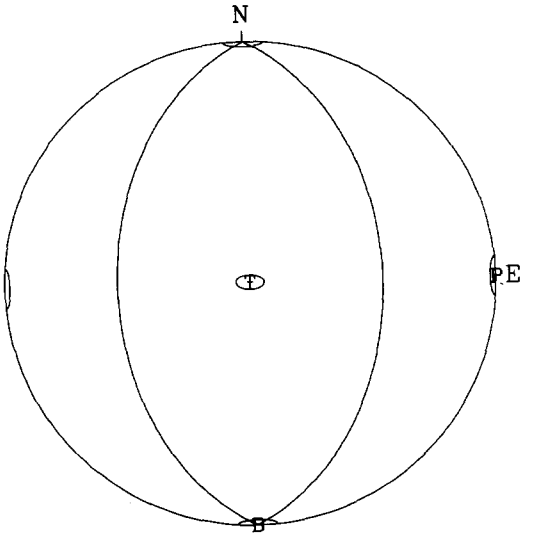

Fig. 7. Nodal-plane solutions for the simple-source data set with a source depth of 33 km. Curves surrounding the P, T and B axes represent 2σ error ellipses.

there are errors in the Green's functions due to the use of a slightly incorrect Earth model.

5.2. *Complex sources*

As in the previous Section, the synthetic seismograms were inverted both with and without the constraint that the source be a point in time. In this Section, however, we wish to discover whether inversion for the optimum point-source solution (in space and time) yields the correct "average" model with the correct scalar moment. We also wish to examine the solutions for finite source duration and investigate what can be learned from the misfits to the data.

The model used to compute the synthetic waveforms was a double source: the first subevent was a thrust event striking due north and dipping 45° to the east, with a scalar moment of 10^{25} dyne cm; the second subevent was the same as the first but with a dip of 75° and a time delay of 10 s. The far-field source vectors for the two subevents are

$$\mathbf{m}_1(t) = (1.0, 0.0, 0.0, 0.0, 0.0, -1.0) \times \delta(t) \times 10^{25} \text{ dyne cm}$$

$$\mathbf{m}_2(t) = (0.5, 0.0, 0.0, 0.866, 0.0, -0.5) \times \delta(t - 10) \times 10^{25} \text{ dyne cm}$$

Using very long-period data, such as IDA or low-pass filtered SRO data, for which there is not sufficient resolution to detect the complex nature of such an event, the result of a linearized inversion should be a combination of the two sources approximated by

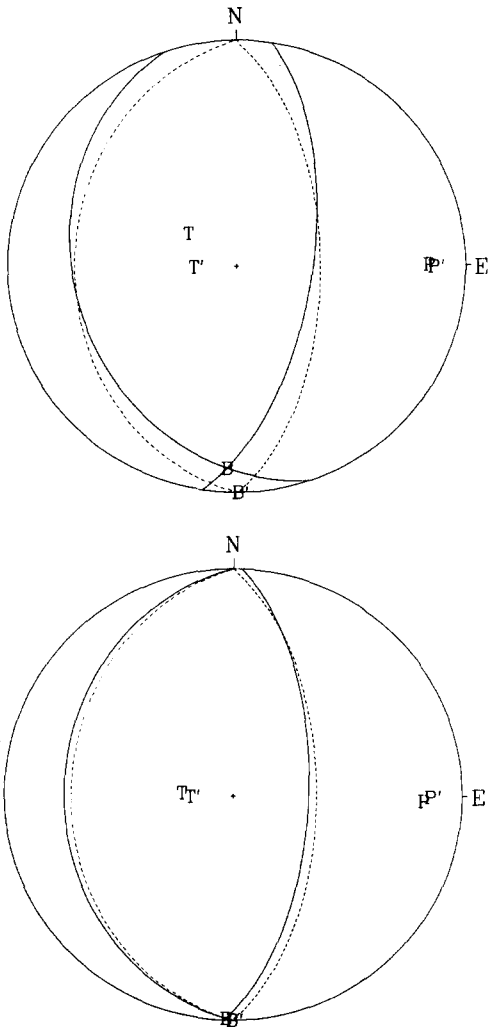

Fig. 8. Nodal-plane solutions for the complex-source data sets obtained by decomposition of the moment-tensor solutions. Conventions as in Fig. 3: (a) source depth 33 km; (b) source depth 520 km.

$$\mathbf{m}(t) = (1.5, 0.0, 0.0, 0.866, 0.0, -1.5) \times 10^{25} \text{ dyne cm}$$

This represents a thrust event striking due north and dipping 60° to the east, with a scalar moment of 1.7×10^{25} dyne cm. A desirable feature of the signal-enhancement algorithm would be to retrieve this solution when constraining the source to be a point in time. As shown in Table II and Fig. 8 this is almost the case. Essentially correct orientations are retrieved; however, the scalar moments returned are underestimated by a factor of 2 when the correct source depths are used to compute the Green's functions. A comparison between the data and the synthetic seismograms obtained when the shallow (33 km) complex solution was inverted with the constraint that the solution be a point in time is shown in Fig. 9.

The unconstrained solutions reveal this to be a multiple event with a peak in the moment rate tensor at $t = 0$ and another peak at $t = 10$ s. Owing to the lack of resolution, the second peak in the moment rate tensor is fairly broad, and the nature of the source is better distinguished in the moment tensor as a function of time. The cumulative solutions are shown in Table II, where it can be seen

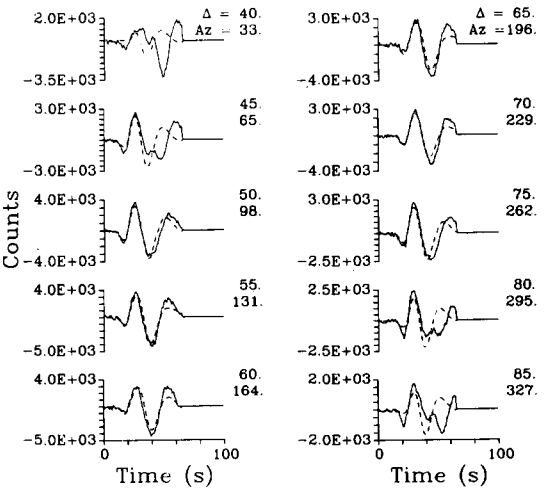

Fig. 9. Comparison of the original complex-source data set for an event 33 km deep (solid lines) and the synthetic seismograms (dashed lines) obtained when these data are inverted using the multichannel signal-enhancement algorithm with the constraint that the solution be a point in time.

that both the total scalar moment and the source orientations are very close to those expected. The migrations resulting from decomposing the moment tensors into their principal axes for each point in time are shown in Fig. 10. The positions of the principal axes as functions of time are also very close to those expected. The motion of the axes, however, occurs not in discrete jumps but is smoothed out, owing to the lack of resolution.

Finally, the power of the deconvolution method is shown by this example. The primary averaging functions and the model averages obtained for the shallow (33 km) event are shown in Fig. 11. There are two peaks resolved, one at $t = 0$ and one at $t = 10$ s. The peaks are clearly simple replications of the averaging functions, so the spike-fitting

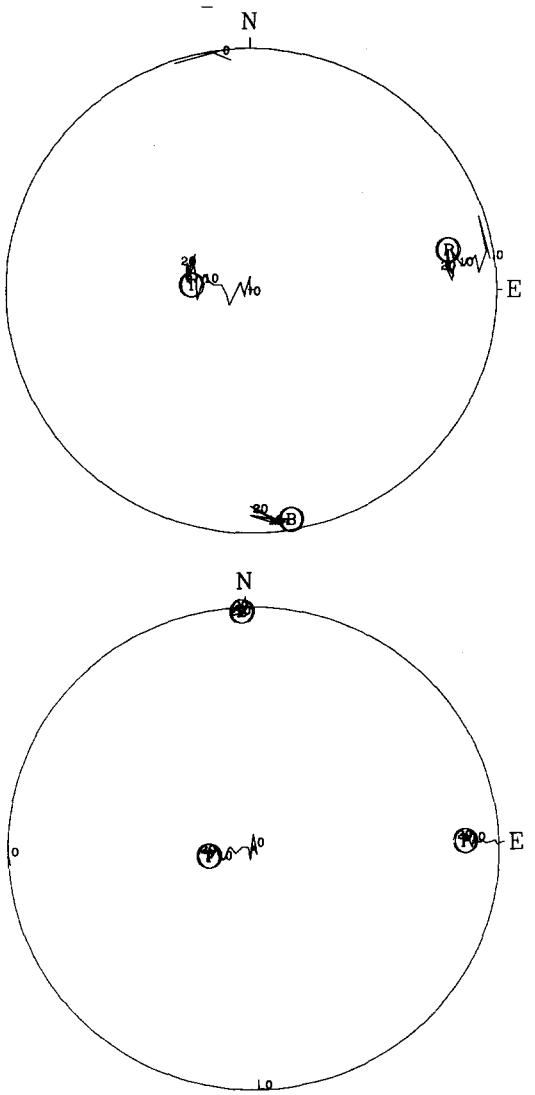

Fig. 10. Principal axes as functions of time for the complex-source data sets obtained by decomposition of the moment-tensor solutions. Conventions as in Fig. 4: (a) source depth 33 km; (b) source depth 520 km.

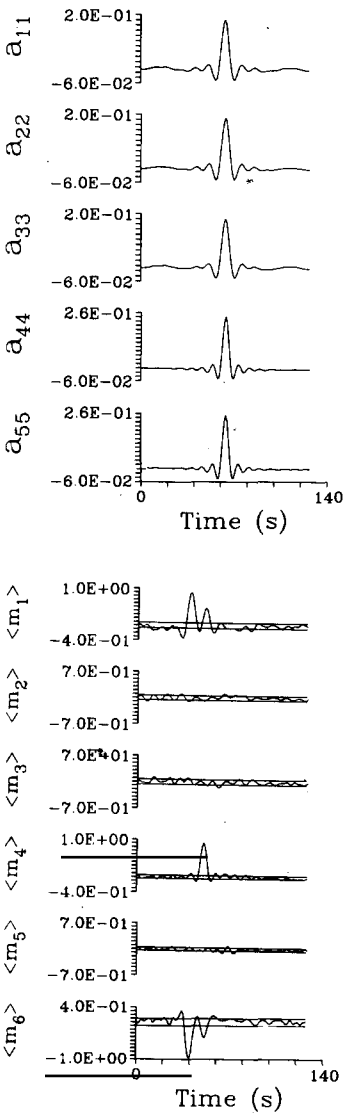

Fig. 11. (a) Primary averaging functions and (b) moment-rate-tensor averages for the complex-source data set with a source depth of 33 km. Horizontal lines indicate $\pm 1\sigma$ levels.

TABLE III

Complex-source double-couple parameters: deconvolution method

	Scalar moment ($\times 10^{25}$)	Strike (deg.)	Dip (deg.)	Slip (deg.)	P		T		B		Misfit [a]
					Az. (deg.)	Plunge (deg.)	Az. (deg.)	Plunge (deg.)	Az. (deg.)	Plunge (deg.)	
Correct solution											
(1) $t=0$	1.0	0	45	90	90	0	0	90	0	0	–
(2) $t=10$	1.0	0	75	90	90	30	270	60	0	0	
True source depth = 33 km											
$h=33$											
(1) $t=0$	0.9	0	45	90	90	0	0	90	0	0	0.080/0.088
(2) $t=11$	0.9	0	78	90	90	33	270	57	0	0	
$h=44$											
(1) $t=0$	0.9	0	45	90	90	0	0	90	0	0	0.339/0.056
(2) $t=11$	1.0	302	66	120	11	16	253	58	109	27	
True source depth = 520 km											
$h=520$											
(1) $t=0$	0.9	0	45	90	90	0	0	90	0	0	0.076/0.083
(2) $t=10$	1.1	0	77	90	90	32	270	58	0	0	
$h=532$											
(1) $t=0$	0.9	0	45	90	90	0	0	90	0	0	0.080/0.083
(2) $t=11$	1.0	0	78	90	90	33	270	57	0	0	

[a] $\chi/E[\chi]$.

method discussed previously may be used. The results indicate that the event is composed of two discrete subevents; the double-couple parameters are shown in Table III. When the spikes are convolved with the Green's functions the "synthetic" data set is produced. The comparison between this and the original data for the shallow event is shown in Fig. 12. For this event, the use of Green's functions for a source depth of 44 km resulted in an unreliable solution ($E[\chi] = 0.06$, $\chi = 0.34$). Also, the averages obtained were oscillatory, which indicated that the procedure had not worked well. However, varying the assumed source depth would eventually yield the proper solution. For the deep (520 km) event, assuming a source depth of 532 km once again resulted in an essentially correct solution but with a slightly greater misfit to the data.

In these tests the amount of misfit is diagnostic not only of the wrong source depth being assumed, but also of the complexity of the event. For the simple sources (Table I) it can be seen that inverting with a finite-duration time function only slightly improves the misfit. However, in Table II the misfits for the finite-duration solutions are improved by more than an order of magnitude. This is a clear indication of source complexity.

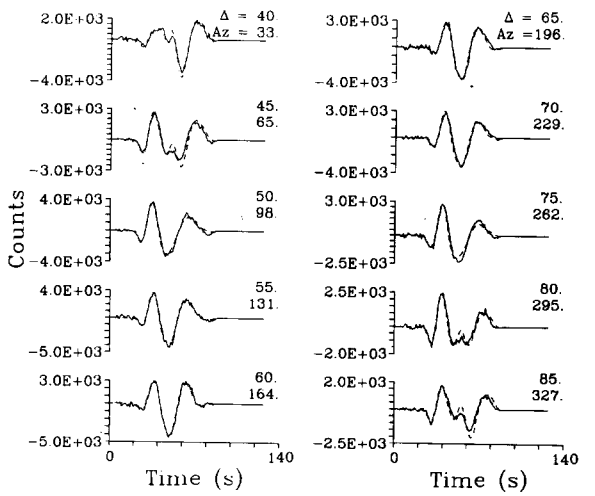

Fig. 12. Comparison of the original complex-source data set for an event 33 km deep (solid lines) and the convolution of the multichannel vector-deconvolution results with the Green's functions (dashed lines).

Furthermore, when inverting the simple events there is essentially no CLVD component in the solutions, whereas for the complex sources there are significant (~ 10%) CLVD components present when the source is constrained to be a point in time when using the multichannel signal-enhancement algorithm. When the inversion is done using the deconvolution algorithm, the complexity of the source may be discerned from an examination of the number and widths of the peaks resolved in the model averages.

6. Discussion

Both of the algorithms presented give good results in the synthetic tests and, more importantly, seem also to work well when applied to real data (Fig. 13, and Sipkin, 1981). Each algorithm has different advantages and disadvantages and is, in certain ways, complementary to the other. The multichannel signal-enhancement method, once the data have been reviewed for unusable waveforms, is almost entirely automatic and involves no further decision-making. Its major disadvantage is that, being a "construction" method, it is difficult to obtain formal estimates of the statistics for the final results. Furthermore, there is the question of the uniqueness of the solution, although tests using both synthetic and real data indicate that this is probably not a problem. Both of these issues are resolved by using the multichannel vector-deconvolution method. The major disadvantage of this method is that it requires a certain amount of interaction with the operator, and is not as objective. First, a value for the weights must be chosen which will sufficiently annihilate the secondary averaging functions; then the "optimum" point on the trade-off curve must be determined; and finally, the number of peaks resolved must be decided. However, these decisions which must be made are relatively simple and straightforward, and the entire process does not take long to complete.

Both of the procedures are robust with respect to minor errors in the Green's functions, and thus any errors in the Earth model or in the hypocentral location, within the typical error bounds,

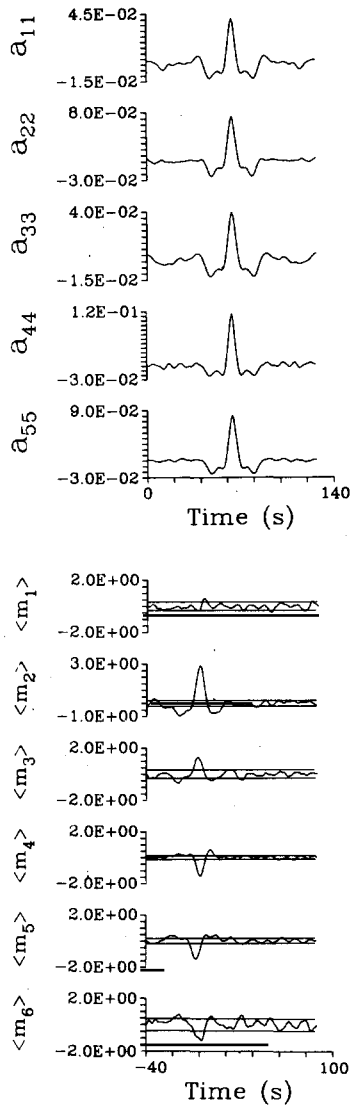

Fig. 13. (a) Primary averaging functions and (b) moment-rate-tensor averages for a deep event (depth = 532 km) in the Banda Sea region ($m_b = 5.8$) on June 11, 1980.

will not adversely affect the solutions. Furthermore, the misfits to the data may be used to refine estimates of the source depth.

One of the "hidden" advantages of using a least-squares fitting criterion is that features in the waveforms which are coherent across the suite of seismograms will be fitted preferentially over features that are not. The result of this, when inverting real data, is that the first few cycles of the waveform will usually be fitted better than the later part. Since the first portion of the waveform is probably more sensitive to the source, and the later parts may contain the effects of reverberations and other structural influences, this is a desirable aspect. Smaller misfits could be obtained by including such structural effects in the Green's functions, but this would require a knowledge of the crustal and upper-mantle structure beneath each station. However, since these effects are de-emphasized by the fitting procedures, this is not really necessary.

It should be pointed out that when inverting entire waveforms for the optimum point source in space and time, the resulting solution will be an average over the spatio–temporal dimensions of the true source. Thus the solution will not necessarily correspond to a fault-plane solution determined by fitting first-motion data, which represents the source orientation at the initiation of rupture. Furthermore, for a complex event, some of the synthetic seismograms for the "average" source may have first motions which disagree with the data. By using solutions which represent different frequencies and different portions of the seismogram it may be possible to map out the rupture history of a complex event.

Acknowledgments

I would like to thank Doug Oldenburg, Bruce Julian, Ray Buland and George Choy for many helpful discussions. In addition, I would like to thank Doug Oldenburg for supplying some of his software, and Ray Buland and George Choy as well as two anonymous reviewers for suggesting numerous improvements to the manuscript. Finally, I would like to thank Madeleine Zirbes for her aid in retrieving the data and in preparing the manuscript.

References

Aki, K. and Patton, H., 1978. Determination of seismic moment tensor using surface waves. Tectonophysics, 49: 213–222.

Aki, K. and Richards, P.G., 1980. Quantitative Seismology, Vol. 1. W.H. Freeman, San Francisco, 557 pp.

Backus, G. and Gilbert, F., 1970. Uniqueness in the inversion of inaccurate gross earth data. Philos. Trans. R. Soc. (London), Ser. A, 266: 123–192.

Buland, R. and Gilbert, F., 1976. Matched filtering for seismic moment tensor. Geophys. Res. Lett., 3: 205–206.

Chapman, C.H., 1978. A new method for computing synthetic seismograms. Geophys. J., R. Astron. Soc., 54: 481–518.

Claerbout, J.F., 1976. Fundamentals of Geophysical Data Processing. McGraw-Hill, New York, 274 pp.

Dey-Sarkar, S.K. and Chapman, C.H., 1978. A simple method for the computation of body-wave seismograms. Bull. Seismol. Soc. Am., 68: 1577–1593.

Dziewonski, A.M., Chou, T.-A. and Woodhouse, J.H., 1981. Determination of earthquake source parameters from waveform data for studies of global and regional seismicity. J. Geophys. Res., 86: 2825–2852.

Engdahl, E.R. and Kanamori, H., 1980. Determination of earthquake parameters. Eos, 61: 62–64.

Fitch, T.J., McCowan, D.W. and Shields, M.W., 1980. Estimation of the seismic moment tensor from teleseismic body wave data with applications to intraplate and mantle earthquakes. J. Geophys. Res., 85: 3817–3828.

Gilbert, F., 1971. Excitation of the normal modes of the earth by earthquake sources. Geophys. J., R. Astron. Soc., 22: 223–226.

Gilbert, F. and Dziewonski, A.M., 1975. An application of normal mode theory to the retrieval of structural parameters and source mechanisms from seismic spectra. Philos. Trans. R. Soc. (London), Ser. A, 278: 187–269.

Kanamori, H. and Given, J.W., 1981. Use of long-period surface waves for fast determination of earthquake source parameters. Phys. Earth Planet. Inter., 27: 8–31.

Langston, C.A., 1981. Source inversion of seismic waveforms: the Koyna, India earthquakes of 13 September 1967. Bull. Seismol. Soc. Am., 71: 1–24.

McCowan, D.W., 1976. Moment tensor representation of surface waves. Geophys. J., R. Astron. Soc., 44: 595–599.

Mendiguren, J.A., 1977. Inversion of surface wave data in source mechanism studies. J. Geophys. Res., 82: 889–894.

Oldenburg, D.W., 1981. A comprehensive solution to the linear deconvolution problem. Geophys. J., R. Astron. Soc., 65: 331–357.

Oldenburg, D.W., 1982. Multichannel appraisal deconvolution. Geophys. J., R. Astron. Soc., 69: 405–414.

Oppenheim, A.V., 1978. Applications of Digital Signal Processing. Prentice–Hall, Englewood Cliffs, NJ, 499 pp.

Robinson, E.A., 1967. Multichannel Time Series Analysis with Digital Computer Programs. Holden–Day, San Francisco, 298 pp.

Sipkin, S.A., 1981. Determination of seismic source parameters from the inversion of waveform data. Eos, 62: 950.

Strelitz, R.A., 1980. The fate of the downgoing slab: a study of the moment tensors from body waves of complex deep-focus earthquakes. Phys. Earth Planet. Inter., 21: 83–96.

Stump, B.W. and Johnson, L.R., 1977. The determination of source properties by the linear inversion of seismograms. Bull. Seismol. Soc. Am., 67: 1489–1502.

Ward, S.N., 1980a. Body wave calculations using moment tensor sources in spherically symmetric, inhomogeneous media. Geophys. J., R. Astron. Soc., 60: 53–66.

Ward, S.N., 1980b. A technique for the recovery of the seismic moment tensor applied to the Oaxaca, Mexico earthquake of November 1978. Bull. Seismol. Soc. Am., 70: 717–734.